A luminescent Poly(amidoamine)-Iridium complex as a new singlet-oxygen sensitizer for photodynamic therapy

*Daniela Maggioni,[#&‡] * Marco Galli,[#] Laura D'Alfonso,[§] Donato Inverso,[†] Maria Vittoria Dozzi,[#] Laura Sironi,[§] Matteo Iannacone,[†] Maddalena Collini,[§] Paolo Ferruti,[#&] Elisabetta Ranucci,[#&] Giuseppe D'Alfonso[#&]*

[#] Dipartimento di Chimica, Università degli Studi di Milano, Via Golgi 19, 20133 Milano, Italy

[§] Dipartimento di Fisica, Università di Milano Bicocca, Piazza della Scienza 3, 20126 Milano, Italy

[†] Division of Immunology, Transplantation and Infectious Diseases, Dynamics of Immune Responses Unit, San Raffaele Scientific Institute, Via Olgettina 58, 20132 Milano, Italy and Vita-Salute San Raffaele University, Via Olgettina 58, 20132 Milano, Italy

[&] Milan Research Unit of Consorzio INSTM, Via Golgi 19, 20133 Milano, Italy

[‡] ISTM, CNR, via Golgi 19, 20133 Milano, Italy

KEYWORDS: Photodynamic therapy, Iridium, poly(amidoamine)s, luminescence, singlet oxygen, two-photon excitation

ABSTRACT

A polymer complex (**1P**) was synthesized, by binding bis(cyclometallated) $Ir(ppy)_2^+$ fragments (ppy = 2-phenylpyridyl) to the phenanthroline (phen) pendants of a poly(amidoamine) copolymer (PhenISA, in which the phen pendants involved ca. 6% of the repeating units). The corresponding molecular complex $[Ir(ppy)_2(bap)]^+$ (**1M**, bap = 4-(butyl-4-amino)-1,10-phenanthroline) was also prepared for comparison. In water solution **1P** gives nanoaggregates with hydrodynamic diameter of 30 nm, in which the lipophilic metal centers are supposed to be segregated within polymer tasks, to reduce interaction with water. Such confinement, joined to the dilution of the triplet emitters along the polymer chains, led to higher photoluminescence quantum yield for **1P** with respect to **1M** (0.061 *vs.* 0.034 in aerated water solution), with longer lifetime of the ^{3}MLCT excited states and blue shifted emission (595 nm vs. 604 nm). The NMR data supported the segregation of the metal centers. The photoreaction of O_2 with 1,5-dihydroxynaphthalene showed that **1P** is able to sensitize $^1O_2$ generation, but with halved quantum yields with respect to **1M**. Cellular uptake experiments showed that both **1M** and **1P** are efficient cell staining agents endowed with two-photon excitation (TPE) imaging capability. TPE microscopy at 840 nm indicated that both the complexes penetrate the cellular membrane of HeLa cells, locating in the perinuclear region. Cell PDT tests showed that both **1M** and **1P** are able to induce cell apoptosis upon Xe lamp irradiation. The fraction of apoptotic cells was higher for **1M** than for **1P** (74% for **1M**, 38% for **1P**, 6 h after irradiation for 5 min), but cells incubated with **1P** showed much reduced necrosis and also a lower toxicity in the absence of irradiation. More generally, the results evidenced that the cell damage induced by **1M** was avoided by binding the Ir sensitizers to the poly(amidoamine).

1. INTRODUCTION

Photodynamic therapy (PDT)[1] is receiving increasing attention as non-invasive clinical treatment for different types of cancer[2] (such as those affecting skin,[3] bladder,[4] esophagus,4 lung,[5] head and neck)[6] and as alternative method of killing pathogens in localized infections.[7]

PDT is based on the use of a photosensitizer (PS), which efficiently populates an excited triplet state upon interaction with visible light. The triplet state of the PS (^{3}PS*) can produce toxic reactive oxygen species (ROS), such as singlet oxygen ($^1O_2$) or free radicals, by two different pathways. Actually ^{3}PS* can react with other molecules, giving intermediate free radicals, that finally generate ROS (type I photochemistry). Otherwise, it can directly interact with molecular oxygen in its ground triplet state, producing "in situ" cytotoxic singlet oxygen ($^1O_2$), through an energy transfer process (equation 1).

$$^3PS^* + {}^3O_2 \rightarrow PS + {}^1O_2 \qquad (1)$$

This type II photochemistry is the most relevant mechanism for PDT in cells, since most PSs are effective $^1O_2$ producers. The generated reactive oxygen species are capable of causing irreversible damage, if generated inside cells, and in particular inside some specific subcellular organelles (mitochondria, Golgi apparatus etc.), where the PS localizes and accumulates. Indeed, singlet oxygen has a radius of destruction measured in nanometers (10 ÷ 60 nm, its lifetime being in the range 10 ÷ 320 ns), and then the photodynamic damage will occur only very close to the intracellular location of the PS.[8] In dependence of many factors, one of which is the subcellular location of the PS, PDT treatment will cause cell death by apoptotic or necrotic pathways. Apoptosis is a programed cell death that does not cause inflammation in vivo, while necrosis is a pathological cell death, where cellular content leaks out, potentially causing lethal damage in cells nearby and inflammation in vivo. It was found that in many cases PDT is highly efficient in inducing apoptosis, as the result of a complex cascade of events.[8,9] This feature is

very important, since it implies that lower doses than those needed to produce necrosis may be effective in cell killing.[10] Furthermore, the efficient induction of apoptosis by PDT implies that PDT may be able to bypass mechanisms that make cells resistant to apoptosis in response to chemotherapeutic drugs and ionizing radiation.[10]

PDT would therefore selectively kill diseased cells, reducing collateral effects on healthy tissues, provided that selective delivery of the PS to the target was assured. Porphyrins,[1a,11] phthalocyanines,[1a] fullerene derivatives,[12] and organic dyes, like methylene blue[13] or rose Bengal,[14] can be mentioned as valid PSs, as well as organometallic complexes.[1a] Among them, cyclometalated iridium complexes have attracted much attention[15,16,17] due to many favorable properties: high quantum yields of triplet formation (even higher than 0.9 in deaerated solutions),[18] long lifetimes of the excited triplet state (usually in the microsecond range, long enough to enable quenching reactions with $^3O_2$ before spontaneous decay), triplet energy high enough to allow the energy transfer process (equation 1). Moreover, it has been shown that they are usually resistant to attack by singlet oxygen.[16]

However, several disadvantages hinder biomedical applications of these complexes. Their solubility in water media is generally very low. Moreover, the circulating time of small molecules in biological fluids is generally too short to allow significant accumulation of the molecular sensitizer in proximity of the target in *in-vivo* applications.

The loading of complexes on suitable nanometric carriers can be exploited to improve the solubility in aqueous media, increase the plasma residence time, and reduce the toxicity.[1b,19] Actually stealth nanoparticles (i.e. nanoparticles covered by macromolecules making them invisible to the Reticulo endothelial system) can benefit of a prolonged circulating time and effectively accumulate into solid tumors, owing to the enhanced permeability and retention (EPR) effect.[20]

Linear amphoteric poly(amidoamines) (PAAs)[21] have well established properties of water solubility, biocompatibility, biodegradability and stealth-like behavior.[22] Moreover, they tend to aggregate in water solution in the form of small nanoparticles, with hydrodynamic diameters in the range of 5-20 nm.[23, 24] They are therefore very attractive as carriers for molecular complexes. In a previous work a PAA copolymer (PhenISA, Chart 1) was synthesized bearing phenanthroline (phen) pendants,[24] which are strong chelating ligands towards a variety of transition-metal fragments. The phen ligand pendants involved about 6% of the repeating units, whereas the large majority of the units were those of the ISA23 polymer.[25] PhenISA was able to bind $Re(CO)_3^+$ or $Ru(phen)_2^{2+}$ fragments, affording luminescent polymer complexes, which were internalized by HEK-293 cells.[24] These results prompted us to investigate the binding to PhenISA of iridium fragments, in order to obtain a luminescent triplet emitter useful both for optical imaging and for producing $^1O_2$ for PDT purposes.

This paper reports on the synthesis of a water-soluble Ir-PhenISA conjugate and its photochemical characterization, showing that the binding to the polymer improved the photophysical properties of the Ir emitters. The photoxidation of 1,5-dihydroxynaphthalene (DHN) was used to check the capability of this new metallo-polymer to act as sensitizer of $^1O_2$ generation. In preliminary tests with HeLa cells the complex was internalized in cells and could be imaged by two-photon excitation microscopy. Moreover, the complex was able to induce cell apoptosis upon Xe lamp irradiation, with no evidence of the intrinsic cell damaging properties shown by the corresponding Ir free complex.

Chart 1. A sketch of the PhenISA copolymer.

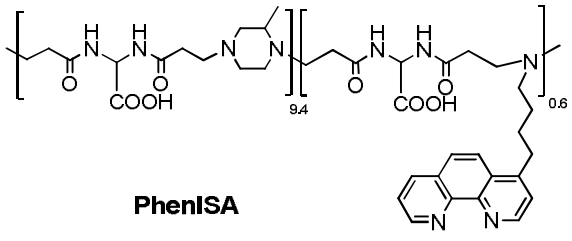

PhenISA

2. RESULTS AND DISCUSSION

2.1. The model complex $[Ir(ppy)_2(bap)]^+$ ($\mathbf{1_M}$) (ppy = 2-phenylpyridyl, bap = 4-(butyl-4-amino)-1,10-phenanthroline). The related $[Ir(ppy)_2(phen)]^+$ complex was previously prepared by reacting the dinuclear precursor $[Ir(ppy)_2Cl]_2$ with phen, at high temperature in ethylene glycol.[26] In the polymer complex here reported the phen ligands are appended to the polymer chain by the butylamino substituents in the 4-position of the phenanthrolines (bap ligand, whose synthesis has been reported elsewhere).[24,27] It was therefore necessary to synthetize the $[Ir(ppy)_2(bap)]^+$ complex ($\mathbf{1_M}$), in order to have a reliable molecular model of the designed polymer complex. The literature route was followed, with some modifications (Scheme 1). The precursor $[Ir(ppy)_2Cl]_2$ was treated with two equivalents of bap ligand in a mixed solvent (THF/H_2O 1:1) under mild heating (ca 70 °C). A clear yellow solution formed upon heating and the orange photoluminescence of the Ir complex progressively overcame the blue fluorescence of free phen. The reaction progress was monitored by ^1H NMR spectroscopy. All the resonances were attributed by scalar and dipolar correlation 2D ^1H-^1H and ^1H-^{13}C NMR experiments (see Figures S1-S3 in Supporting Information, SI).

Scheme 1. The synthesis of the complex $\mathbf{1_M}$.

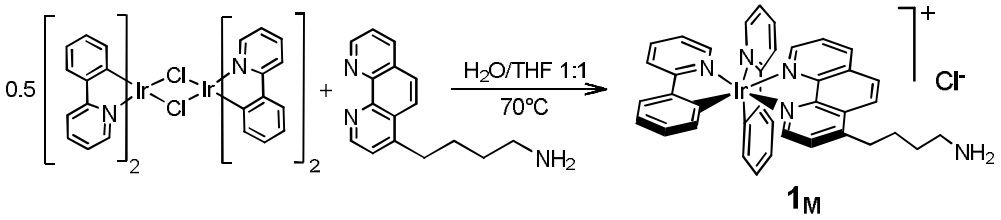

At variance with the $[Ir(ppy)_2(phen)]^+$ complex, $\mathbf{1_M}$ (as chloride salt) is moderately soluble in water, due to the presence of the protonated amino group on the phen ligand (pK_a = 10.2, as determined by potentiometric titration on the bap ligand). The solubility was high enough to allow performing the photophysical characterization in water solution, as well as the biological tests described in Section 2.5. However, a minor fraction of the compound was found (by DLS and NMR data) to be present in the form of nanoaggregates, as discussed below.

The UV-Vis absorption spectrum (Figure 1) of $\mathbf{1_M}$ shows strong spin-allowed ligand-centered (^{1}LC) bands, in the range 200-300 nm, and broad weaker absorptions at longer wavelengths (peaks are recognizable at ca. 378 nm and 417 nm, Figure 1, whose position did not change significantly on varying the solvent, see Figure S4), attributable to singlet metal-to-ligand charge transfer transitions (^{1}MLCT), in agreement with literature data for similar complexes.[15,26,28]

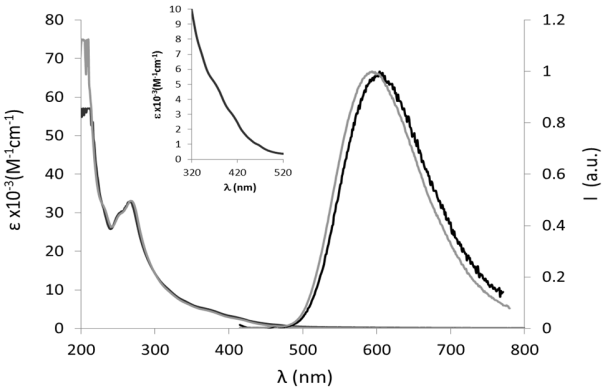

Figure 1. UV-Vis absorption (left) and photoluminescence (right) spectra of $\mathbf{1_M}$ (black traces) and $\mathbf{1_P}$ (gray traces) (water solution, room temperature, λ_{ex} = 400 nm).

Upon excitation at 400 nm, complex $\mathbf{1_M}$ exhibits yellow-orange photoluminescence, at wavelengths that are strongly sensitive to the nature of the solvent (Table 1, Figure S4 in SI). A blue shift is observed on decreasing solvent polarity,[29] as it is typical of excited states more polar than the ground ones (such as CT states), which are preferentially stabilized by polar solvents, provided the excited state lifetime is longer than the solvent reorganization time.[32,33] The sharp drop of lifetimes (τ) and photoluminescence quantum yields (PLQYs, Φ) in the presence of oxygen, observed in CH_2Cl_2 or CH_3CN solution (Table 1) indicates that the emission occurs form an excited state with a substantial triplet nature. This agrees with literature data that attributed the emission from $[Ir(ppy)_2(phen)]^+$ complexes (phen indicating different phenanthroline-based ligands) as arising from ^{3}MLCT states involving the π^* orbitals of phen ligand as the acceptor orbitals.[26,28,34]

In water solution $\mathbf{1_M}$ shows photoluminescence centered at 604 nm, whose position did not change in the pH range 3.2 – 7.2. The behavior in the presence of oxygen did not fit with the typical behavior of triplet emitters, observed in the organic solvents. Lifetimes and PLQYs were little affected by the presence of oxygen (Table 1). Moreover, in aerated conditions, the PLQYs in water were higher than in acetonitrile, contrarily to what expected from the polarity trend. A possible explanation was provided by DLS analysis of the water solution (ca. 2×10^{-5} M), that showed the presence of nanoparticles with hydrodynamic diameters of ca. 200 nm. This suggested that $\mathbf{1_M}$ was not completely dissolved and was present, at least in part, in the form of nanosized aggregates. Such aggregates cannot account for the whole amount of $\mathbf{1_M}$ present in solution, since colloids are NMR silent (or give very broad, hardly detectable resonances),[35] whereas sharp ^{1}H NMR signals were observed for samples of $\mathbf{1_M}$ in water (see for instance Figure S1 of SI). It has been shown (see Experimental) that the NMR silent fraction of $\mathbf{1_M}$ in water corresponds to about 25% of the whole sample. Such fraction of aggregated $\mathbf{1_M}$, even if

minor, could dominate the emission features, because the complexes inside the nanoparticles are expected to be more brilliant, being protected from the deactivating action of oxygen and of the polar solvent.[36] Therefore the wavelength, lifetime and PLQYs of the emission, measured in water, should mainly be attributed to the aggregates, with little contribution from the free molecules. Interestingly in water a double exponential model was necessary to describe the lifetime decays (Table 1) in order to achieve a function of merit (chi square) comparable with that obtained for the organic solvents. The main component (longer and very little sensitive to oxygen) is ascribable to the species inside the nanoparticles, while the minor component (shorter and strongly affected by oxygen) is attributable to the free molecules.

Table 1. Photoluminescence data for the molecular complex $\mathbf{1_M}$, in aerated or deaerated solution in different solvents, and for the polymer complex $\mathbf{1_P}$, in aerated water solution (room temperature, λ_{ex} = 400 nm). k_r and k_{nr} indicate the radiative and nonradiative decay constants of the excited states.

Compound	Solvent	λ_{em}/ nm	Conditions	τ / ns	Φ	k_r / s^{-1}	k_{nr} / s^{-1}
$\mathbf{1_M}$	$\mathbf{CH_2Cl_2}$	574	Aerated	153	0.052	3.4×10^5	6.2×10^6
			Deaerated	1123	0.35	3.1×10^5	5.8×10^5
$\mathbf{1_M}$	$\mathbf{CH_3CN}$	591	Aerated	56	0.017	3.1×10^5	1.8×10^7
			Deaerated	858	0.30	3.5×10^5	8.2×10^5
$\mathbf{1_M}$	$\mathbf{H_2O}$	604	Aerated	116 (98%) 2 (2%)	0.033	2.8×10^5 [a]	8.3×10^6 [a]
			Deaerated	134 (95%) 64 (5%)	0.038	2.8×10^5 [a]	7.2×10^6 [a]
$\mathbf{1_P}$	$\mathbf{H_2O}$	595 nm	Aerated	212	0.061	2.9×10^5	4.5×10^6

[a] Computed on the most significant lifetime component

2.2. Preparation and characterization of the $\mathbf{1_P}$ complex. The synthesis of the PhenISA copolymer (Chart 1) has been already reported.[24] Its majority part derives from the Michael addition reaction between piperazine and bis(acrylamido)acetic acid (BAC), while the minority

part (ca. 6%) arises from the analogous reaction between BAC and the primary amine bap. Dynamic Light Scattering (DLS) measures indicated that this copolymer in aqueous media self-assembled, giving rise to the formation of roughly spherical nano-aggregates with a hydrodynamic diameter of ca. 20 nm.[24]

Scheme 2. The synthesis of the polymer complex $\mathbf{1_P}$.

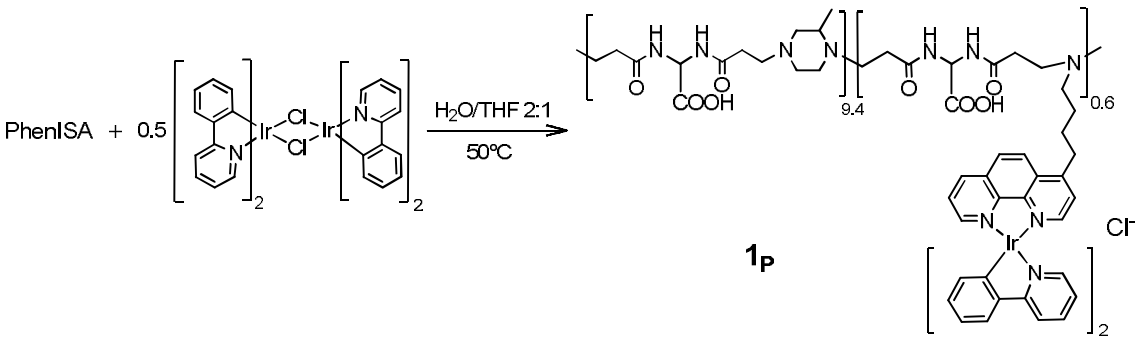

The complexation of Ir to PhenISA was performed by a route similar to that used for preparing the molecular complex $\mathbf{1_M}$ (Scheme 2), in a THF/H_2O mixed solvent containing a double amount of water with respect to the synthesis of $\mathbf{1_M}$, due to the low solubility of PhenISA in non-aqueous media. On the other hand, the presence of THF was necessary because the starting reagent $[Ir(ppy)_2Cl]_2$ is definitely insoluble in water. The reaction temperature was lower (50°C) than that used for the synthesis of $\mathbf{1_M}$, to avoid thermal degradation of the polymer. After 6.5 h the mixture was concentrated under reduced pressure, to remove most of THF, and dialyzed against water for 4 days, to remove unreacted metal fragments and lower MW polymer fractions, if present.

The content of Ir bound to the polymer was measured by ICP-AES analysis. The result (2.45% w/w) indicated that the large majority (88.3%) of the phenanthroline pendants had reacted with $Ir(ppy)_2$ fragments.

The binding of the metal centers did not hamper the tendency of PhenISA to self-aggregate. A DLS measure, performed on a sample of dialyzed and lyophilized **1P**, showed a size distribution centered at ca. 30 nm (Figure S5 in SI), slightly larger than that of PhenISA alone.

Another interesting feature of the organization of the polymer coils in solution was revealed by the ^{1}H NMR spectra of the purified polymer complex **1P** in D_2O solution. In these conditions the aromatic resonances of the ppy and phen ligands were particularly broad, and their integrated intensities did not reflect the true percentage of the minority part of the copolymer (see the bottom spectrum of Figure S6 in SI, in which the aromatic signals are almost undetectable). Progressive addition of THF-d_8 to the NMR tube led to the recovery of the aromatic resonances in their correct intensity (Figure S6 in SI). This suggests that in water solution the complexes, in which the metal is surrounded by the lipophilic cage formed by the three large aromatic ligands, tend to segregate within the polymer to avoid the contact with water. Upon addition of the less polar THF solvent, segregation is relieved, and exposure to the mixed solvent makes the $Ir(ppy)_2(bap)$ pendants more mobile and consequently their ^{1}H signals more visible.

The UV-Vis absorption spectrum of **1P** was superimposable on that of the molecular complex **1M**, except for the very intense absorption at ca 200 nm due to the amide groups of the polymer (gray trace in Figure 1). The photoluminescence spectrum showed instead some significant differences with respect to **1M**. The emission maximum was blue shifted by 9 nm (250 cm^{-1}), and longer lifetimes (212 ns) and higher quantum yields (0.061) were measured. These findings agree with the idea that in water the pendant Ir complexes are segregated into polymer pockets, in which they experience less polar surroundings (so giving blue shifted emission), and a more rigid environment than in solution. Moreover the emitting Ir centers are very diluted along the polymer chains of **1P**, since the units bearing the phen pendants are a very minor component of the copolymer. This prevents the self-quenching and annihilation effects, which are often

encountered for emission from the triplet state of transition metal complexes in solid or in films at high dopant concentrations,[37] and might also occur in the nanoaggregates formed by $\mathbf{1_M}$ in water. In fact, the best emitting features are often observed in systems where a rigid environment (rigidochromic effect)[38] is joined to a low dopant concentration.[39]

2.3. Photochemical stability of $\mathbf{1_P}$. Photochemical stability tests were carried out to check the robustness both of the iridium complex and of the PAA chain under prolonged irradiation in the presence of O_2. This is indeed a key prerequisite for using the polymer complex as a photosensitizer. $\mathbf{1_P}$ was dissolved in water/methanol (85/15) and the solution was saturated with oxygen by bubbling O_2 for 10 min. The solution was then exposed to visible light (Xenon lamp 150 W, cut-off filter at 390 nm) and UV-Vis absorption spectra were recorded every 30 min for 4 hours (Figure S7 of SI). The superposition of the absorption spectra recorded at different times stated the high photostability of the compound. The same test was also repeated for complex $\mathbf{1_M}$, with analogous results.

2.4. Photoreaction of $\mathbf{1_P}$ and $\mathbf{1_M}$ with 1,5-dihydroxynaphthalene, as reporter of $^1O_2$ formation. To test the capability of $\mathbf{1_M}$ and of $\mathbf{1_P}$ to act as sensitizers for $^1O_2$ generation, photochemical reactions were performed in solutions presaturated with O_2, employing 1,5-dihydroxynaphthalene (DHN) as $^1O_2$ reporter. Indeed it is known that DHN promptly and quantitatively reacts with $^1O_2$ giving 5-hydroxy-1,4-naphthalenedione (juglone, Scheme 3).[15,40]

Scheme 3. The photochemical reaction used to monitor $^1O_2$ formation. Here PS represents the Ir complexes $\mathbf{1_M}$ and $\mathbf{1_P}$.

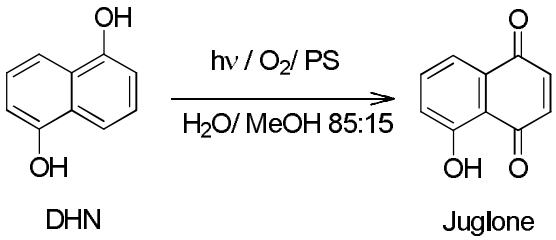

The reaction progress was monitored by UV-Vis absorption spectroscopy, following the decrease of the band at 297 nm due to DHN, and the concomitant increase of the large band centred at 427 nm, due to juglone (Figures 2a and 2b). The reaction occurred without formation of long living intermediates or by-products, as indicated by the two isosbestic points at 280 and 330 nm observed in the spectra recorded during the course of the irradiation. It was checked that in the absence of the Ir sensitizers, juglone formation was negligible, even after 70 min of irradiation of O_2 saturated solutions.

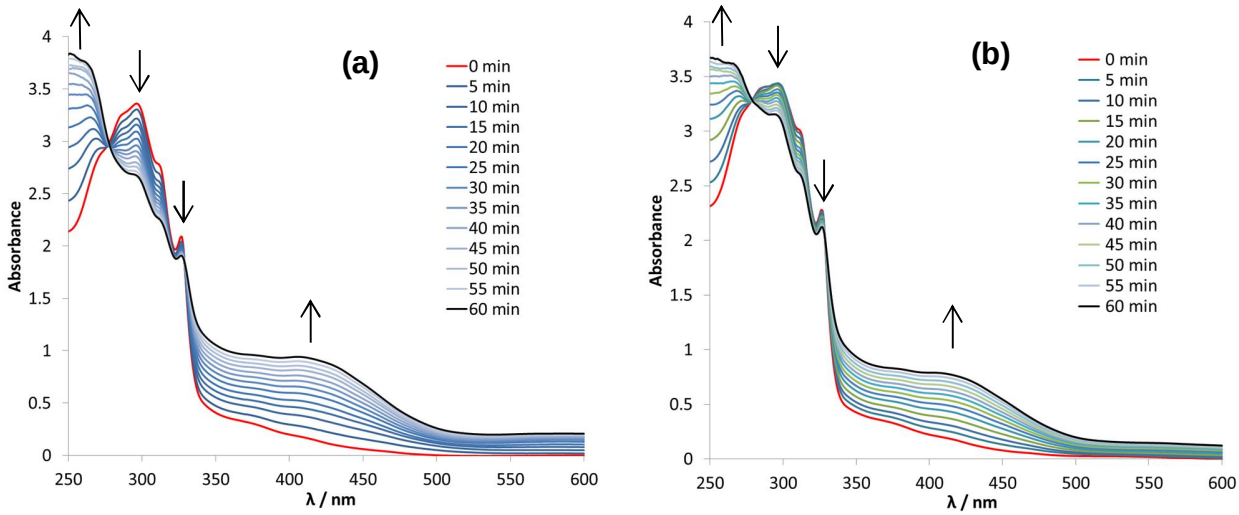

Figure 2. UV-Vis absorption spectra recorded at different times of irradiation (λ > 390 nm, Xenon lamp) on solutions containing DHN (3.7×10^{-4} M) and (a) complex $\mathbf{1_M}$ (4.1×10^{-5} M) or (b) complex $\mathbf{1_P}$ (3.6×10^{-5} mol/L of Ir), in 3 mL of H_2O/MeOH 85/15, bubbled with O_2 for 10 min.

Figure 3 shows the first-order semi-logarithmic plots for reaction 2, sensitized either by $\mathbf{1_M}$ or $\mathbf{1_P}$. In the case of $\mathbf{1_M}$, the values of $\ln(A_t/A_0)$ decreased linearly vs. time, from the very beginning up to ca. 50 min of irradiation, in agreement with a pseudo-first order kinetics, with rate $r = k_{obs}[DHN]$ (slope = $k_{obs} = 5.1\times10^{-3}$ min^{-1}). At longer times progressive deviation from linearity was observed, possibly related to the fact that juglone absorbs at the same wavelengths of the Ir sensitizer. The rate of juglone formation well compares with that observed for the same reaction sensitized by the $[Ir(ppi)_2(phen)]^+$ complex in mixed acetonitrile/2-PrOH solution ($k_{obs} = 6\times10^{-3}$ min^{-1}).[40]

DHN + $^1O_2$ → Juglone + ½ $^3O_2$ (2)

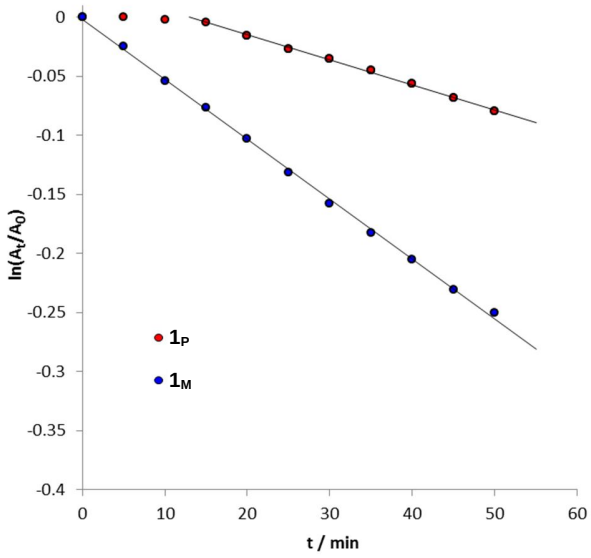

Figure 3. Photooxidation of DHN in the presence of the sensitizers $\mathbf{1_M}$ and $\mathbf{1_P}$ (data until 50 min have been plotted, that corresponds to the linearity time interval). A_t and A_0 represent the absorbance measured at 297 nm (the maximum of the DHN absorption band) at the time t and at the time zero, respectively. The absorbance of the Ir sensitizer at this wavelength was subtracted.

On the contrary for $\mathbf{1_P}$ an induction period was observed, followed by a linear decrease with a lower slope ($k_{obs} = 2.1\times10^{-3}$ min^{-1}). The induction time suggests that at the beginning the polymer

itself competed with DHN for $^1O_2$ consuming, most likely by reaction with the alkene groups,[41] which constitute the terminals of the PAA chains (obtained by Michael addition reactions). Therefore, reaction 2 likely could start only when these terminal groups had been saturated. The lower rate with respect to $\mathbf{1_M}$ is probably attributable to the fact that quenching of excited triplet sensitizers by $^3O_2$ (reaction 1) requires the encounter between the two species, and in $\mathbf{1_P}$ the mobility of the Ir complexes is drastically reduced with respect to $\mathbf{1_M}$ by their binding to the polymer. Furthermore, the photophysical and NMR data suggest that the polymer adopts conformations favoring the segregation of the complex to reduce interaction with water. Therefore the time necessary for the generated $^1O_2$ to diffuse in the solution to encounter the DHN probe must also be considered.

The ratio between the slopes of the two lines reported in Figure 3, corrected to take into account the different amount of radiation absorbed by the two sensitizers during the reaction (see Experimental Section), allowed to estimate the ratio between the quantum yields for $^1O_2$ generation by $\mathbf{1_M}$ and $\mathbf{1_P}$, respectively. A value of 2.1 was obtained (see Experimental Section for details). Binding to the polymer therefore reduces, but not dramatically, the efficiency of the Ir complex as sensitizer for $^1O_2$ generation.

2.5. Cells PDT treatment. Before testing the capability of the Ir complexes to induce cell death by $^1O_2$ generation, their cellular uptake was investigated. The efficiency of incorporation of the photosensitizers into the cells can significantly affect the capability of the sensitizer to induce cell death.[14] Therefore HeLa cells were incubated with compounds $\mathbf{1_M}$ and $\mathbf{1_P}$, at 37 °C under 5% CO_2 atmosphere (see Experimental Section) for different times. Images of the incubated cells were then acquired by two-photon excitation (TPE) microscopy at 840 nm, where both complexes showed the highest two-photon absorption. TPE allows for lower damage of cells and deeper light penetration in vivo, since typical laser wavelengths lie in the range 700-

900 nm, that corresponds to the window where both the tissue chromophores and water absorb more weakly.

Previous studies had shown that cell internalization of the Ru-PhenISA complex required several hours.[24] The uptake of the Ir-PhenISA complex $\mathbf{1_P}$ was therefore checked after 12 h of incubation. On the other hand, the uptake of molecular complexes is usually faster,[42] therefore the internalization of $\mathbf{1_M}$ was monitored after 2 h of incubation.

Figure 4 shows that both the molecular complex $\mathbf{1_M}$ (upper panels) and the polymer complex $\mathbf{1_P}$ (lower panels) are able to penetrate the cellular membrane and tend to locate in the perinuclear region. This is in line with literature data concerning related bis(cyclometallated) Ir complexes, in which localization in subcellular organelles as Golgi apparatus, endoplasmic reticulum, lysosomes or mitochondria was suggested. [17b,d,e, 43]

These preliminary experiments therefore indicated that $\mathbf{1_P}$ is an efficient cell staining agent, endowed with TPE imaging capability, and that it is well tolerated by cells. Indeed cells appeared still viable after the long incubation time, as further confirmed by the quantification of the dead cells on non-irradiated samples, described below.

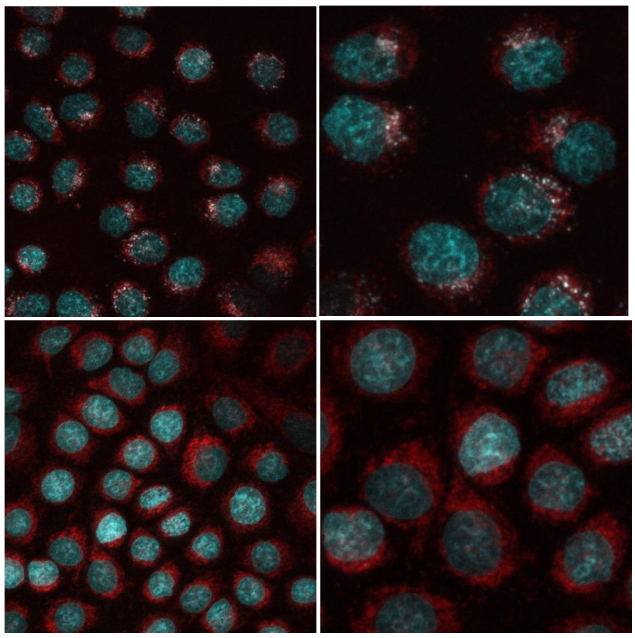

Figure 4. TPE microscopy images (superposition of the blue and the red channels) of HeLa cells incubated for 2 h with 26 μM $\mathbf{1_M}$ (upper panels) or 12 h with 22 μM $\mathbf{1_P}$ (lower panels) and stained with HOECHST to show the nuclei in the blue channel. The red color is due to the Ir complexes. An image of the control HeLa cells (no incubation with the Ir complexes) for this experiment is shown in Figure S8 in SI. Left panels: 157×157 μm^2; right panels: zoom to 79×79 μm^2.

For the PDT tests, HeLa cells were incubated with $\mathbf{1_M}$ or $\mathbf{1_P}$, as described above for the cellular uptake assays. Subsequently, the multiwell plates were irradiated for 5 min with a Xe lamp and then maintained at 37 °C under 5% CO_2 atmosphere (see Experimental Section). The same treatment was applied to control cells (without sensitizer), to check for adverse effect of exposure to the Xe lamp. Cell viability was evaluated by flow cytometry analysis, performed 4 h and 6 h after irradiation (and also on non-irradiated samples, see Figure S9 of SI), using annexin V and 7-aminoactinomycin D (7AAD) staining, to denote apoptotic and necrotic cells, respectively.

Cells incubated with either $\mathbf{1_M}$ or $\mathbf{1_P}$ underwent apoptosis upon irradiation (as shown in Figure 5). The fraction of apoptotic cells was higher for $\mathbf{1_M}$ than for $\mathbf{1_P}$, in line with the kinetics of $^1O_2$ generation measured in the photooxidation of DHN. However, an increased number of necrotic events with respect to the untreated cells was observed in the cells treated with $\mathbf{1_M}$ (Figures 5 and S9).

Next, to investigate the dark toxicity (i.e. toxicity in the absence of irradiation), HeLa cells were incubated with either $\mathbf{1_M}$ or $\mathbf{1_P}$ and the cells viability (number of living cells recovered after treatment) and the number of dead cells were measured (see Experimental Section). As shown in Figure S10, $\mathbf{1_M}$ led to a significantly higher number of dead cells and a significant reduction of cell viability, compared with both untreated and $\mathbf{1_P}$-treated cells.

Therefore, these results, taken together, indicate that the treatment with the free complex $\mathbf{1_M}$ has a significant cytotoxic effect, also without exposure to the Xe lamp. Cells incubated with $\mathbf{1_P}$ showed much reduced cytotoxicity (both in the dark and upon irradiation). In particular, the binding of the sensitizer to the poly(amidoamine) inhibited necrosis upon irradiation, while preserved its ability to induce apoptosis.

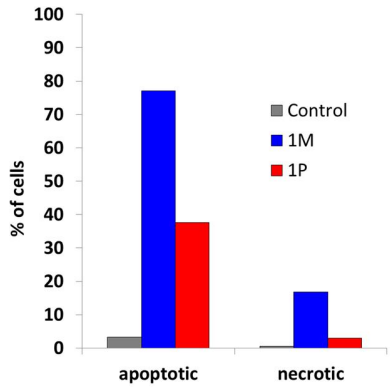

Figure 5. Percentages of dead cells upon PDT treatments (6 h after irradiation for 5 min), in control samples or in samples sensitized by $\mathbf{1_M}$ or $\mathbf{1_P}$, as a result of apoptotic or necrotic events.

3. CONCLUSIONS

The new luminescent metallo-polymer $\mathbf{1_P}$ presented here is of interest in several respects. Upon light absorption the bis(cyclometallated) Ir complexes appended to the polymer give rise to triplet metal-to-ligand-charge-transfer excited states, that can either radiatively decay or react with $^3O_2$, and then can be exploited either for imaging or for PDT applications. It has been found that the photoluminescence can be triggered by two-photon excitation, which offers advantages over traditional one-photon excitation, in terms of lower damage of cells and deeper light penetration in vivo. Moreover preliminary tests on living HeLa cells have shown that $\mathbf{1_P}$ is internalized by cells, which is an important asset for PDT applications. Therefore, from the point of view of the imaging applications, $\mathbf{1_P}$ provides an efficient water-soluble cell staining agent, which also benefits of TPE imaging capability, and that it is well tolerated by cells.

Moreover, the binding to the polymer improved the photophysical properties of the Ir complexes, doubling lifetimes and photoluminescence quantum yields, most likely because the metal centers, buried within the lipophilic ligand cages, are diluted and segregated into polymer tasks, in an environment more rigid and somewhat protected from water (and possibly from O_2). In fact, several examples are reported in the literature, in which similar approaches have been used to shield triplet excited states from quenchers that would prevent applications in bio-imaging or photo-catalysis.[44]

Notably, in the present case the segregation did not hinder the ability of the Ir complexes contained in $\mathbf{1_P}$ to sensitize $^1O_2$ generation. The rate of $^1O_2$ generation was lower for $\mathbf{1_P}$ than for the free complex $\mathbf{1_M}$, as shown by the photooxidation of DHN, but the rate difference was not dramatic. Then $\mathbf{1_P}$ maintained the capability to induce apoptosis, by irradiation for a short time, in a large fraction of the irradiated cells. The percentage of dead cells was lower than that observed in the PDT tests sensitized by $\mathbf{1_M}$, but $\mathbf{1_P}$ caused much reduced necrosis than $\mathbf{1_M}$. Then

the experiments here reported indicate that the binding of the Ir sensitizers to the PhenISA copolymer allows to avoid the significant cell damage caused by the free complex $\mathbf{1_M}$.

This is just one of the beneficial effects expected from the binding of metal emitters to poly(amidoamine)s, whose biocompatibility has been already evidenced.[22] Moreover, for in vivo applications, it is expected that the binding of the sensitizers to a nanometric carrier will increase their circulating time and favor their effective accumulation into solid tumors by the EPR effect.

The present work therefore provides the proof of principle that the binding of Ir triplet emitters to poly(amidoamine)s affords conjugates with potential both as cell imaging agents and as sensitizers of $^1O_2$ generation. For improving such potential, in view of clinical applications, further work will be necessary, to tailor the ligand sphere of the metal and to shed light on the mechanism of cell penetration and on the intracellular localization.

4. EXPERIMENTAL SECTION

4.1. Materials. 2-Methylpiperazine was purchased from Fluka and purified by sublimation, with final purity (98%) determined by acidimetric titration. N,N′-bis(acrylamido)acetic acid (BAC) was prepared following a literature method,[45] and purity (98%) was determined by NMR spectroscopy and titration. $[Ir(ppy)_2Cl]_2$ was prepared by a literature method,[46] using $IrCl_3 \cdot 3H_2O$ as precursor (BASF). All the other reagents were from Aldrich and used as received, if not otherwise specified. THF was distilled from Na/benzophenone using standard Schlenk techniques. Ultrapure water (Milli-Q, Millipore, resistivity = 18 MΩ cm^{-2}) was used for the preparation of the aqueous solutions. D_2O (99.9%) was purchased from Aldrich and used as received, THF-d_8 (99.9%) was purchased from CIL.

4.2. Instruments and Methods. NMR experiments were performed on a Bruker DRX400 spectrometer, equipped with a Bruker 5 mm BBI Z-gradient probe head with a maxima gradient strength of 53.5 G/cm.

DLS measurements were performed using a Malvern Zetasizer nano ZS instrument at 289 K on samples dissolved in ultrapure water (typically 1 mg/mL).

Elemental C, H, N analyses were performed on a Perkin-Elmer CHN 2400 instrument. Ir content was determined by ICP-AES (ICAP 6300, Thermo Electron) on a known amount of $\mathbf{1_P}$ dissolved in 1.5 mL 30% HCl (Suprapur) and 0.5 mL 65% HNO_3 (Suprapur), digested overnight at room temperature and finally diluted to 10 mL with ultrapure water in a volumetric flask.

UV-vis absorption spectra were acquired on an Agilent Model 8543 spectrophotometer at room temperature. The determination of the molar absorptivity (ε) values of the ^{1}MLCT transitions for $\mathbf{1_P}$ was performed by dissolving in a volumetric flask an accurately weighted amount of $\mathbf{1_P}$ (balance with readability up to 0.01 mg) and calculating the Ir content on the basis of the ICP-AES analysis.

Steady-state photoluminescence measurements were performed on a Jobin-Yvon-Horiba Fluorolog spectrometer, correcting the emission spectra for the spectroscopic sensitivity of the photomultiplier tube. Quantum yields were determined by using $[Ru(bpy)_3]Cl_2$ as standard (Φ = 0.04 in aerated water solutions).[47] The values of the radiative constants k_r have been obtained from the Φ/τ ratio, assuming the efficiency of the intersystem crossing process equal to 1.

Lifetimes were measured by frequency-domain methods. A frequency modulated phase fluorometer (Digital K2, I.S.S., Urbana IL) was employed, using a laser diode at 378 nm as an excitation source. At least fifteen data points have been acquired at logarithmically spaced frequencies in the range of 0.3-60 MHz with a cross correlation frequency of 400 Hz. The convenient accuracy for phase angles and modulation ratios was of 0.2° and 0.004, respectively.

Lifetime measurements were performed under the magic angle conditions and a 535 nm long pass filter (Andover Co.) was employed in order to cut light scattering. A solution of glycogen in doubly distilled water was used as reference sample. Lifetime data fitting was accomplished by an I.S.S. routine based on the Marquardt least squares minimization. In the case of multiple exponential components in the decay scheme, the fit of the fluorescence intensity decay F(t) yields the lifetime values τ_i together with the corresponding fractional intensities f_i: $F(t) = \sum\alpha_i e^{-t/\tau_i}$ and $f_i = \alpha_i\tau_i/\sum\alpha_i\tau_i$, where α_i represent the pre-exponential factors. The value of the fractional intensities for each component is proportional to the molar extinction coefficient ε_i, to the concentration c_i and to the quantum yield ϕ_i of the component, $f_i \propto \varepsilon_i c_i \phi_i$.

Typical errors affecting the lifetime measurements are about 5%, with the exception of the longer lifetimes (i.e. > 500 ns), for which the error rises to about 10% due to the non optimal working frequency range available of the amplifiers. In organic solvents, the lifetime decay data were satisfactorily described by a simple single exponential model, the fitting of the data yielding chi-square values of the order of 5 and no trends in the residues plot (the deviation of the chi square from the unity is due mainly to the low performance of the amplifiers at 0.3 MHz, since their working range spans the interval 0.1-300 MHz). As stated in the text, in water a double exponential model had to be assumed to describe the lifetime decay in order to achieve a function of merit (chi square) comparable with that obtained for the organic solvents.

The photochemical stability test and the photoreaction with DHN in presence of $\mathbf{1_M}$ and $\mathbf{1_P}$ employed a Jasco V-650 spectrophotometer. The experiments were performed in a 3 mL quartz cuvette, inserted in a home-made housing consisting in a black box mounted on optical bench. The irradiation source was an Osram, model Powerstar HCI-T, 150 W/NDL lamp, mounted on a Twin Beam T 150 R reflector, mainly emitting visible light above 400 nm, with a small emission in the 350–400 nm range which was eliminated after the location of a 390 nm cut off filter at the

black box entrance (Figure S10 in SI). The lamp and the reactor were separated by a fixed distance of 10 cm. The whole set up was maintained at ambient temperature by a continuous stream of air.

4.3. Synthesis of the model complex [Ir(ppy)$_2$(bap)]Cl ($\mathbf{1_M}$.Cl). In a Schlenk tube 34.7 mg of $[Ir(ppy)_2Cl]_2$ (3.24×10^{-2} mmol) were dissolved in 9 mL of anhydrous and freshly distilled THF. A solution of 4-(butyl-4-amino)-1,10-phenanthroline[24,27] (bap, 16.2 mg, 6.45×10^{-2} mmol) in water (9 mL) was then added at room temperature. The mixture was heated at 70°C. The starting turbid suspension rapidly turned to a clear yellow solution and the color observed under UV irradiation changed from blue (fluorescence of free phen) to orange, following the formation of the luminescent Ir complex. The reaction progress was monitored by ^{1}H NMR spectroscopy. Heating was stopped after 5 h and the mixture was stirred overnight. The solvent was evaporated under vacuum, and the product was isolated by precipitation from THF/Et_2O (1:2), and dried under vacuum. Final treatment of the solid with Et_2O (2 mL x 3) followed by vacuum evaporation to dryness gave **$\mathbf{1_M}$.Cl**. Isolated yield: 69%. UV-Vis data (H_2O), MLCT absorptions: λ_{abs} 378 nm (ε = 4690 M^{-1} cm^{-1}), and 417 nm (ε = 2610 M^{-1} cm^{-1}). ^{1}H NMR (D_2O, 300 K, 9.4 T): δ ppm 8.60 (1H, C*H*(9), dd, J = 8.5, 1.0 Hz), 8.33 (1H, C*H*(5), d, J = 9.5 Hz), 8.30 (1H, C*H*(7), dd, J = 5.2, 1.0 Hz), 8.18 (1H, C*H*(2), d, J = 5.3 Hz), 8.16 (1H, C*H*(6), d, J = 9.5 Hz), 8.02 (2H, C*H*(6'), *pseudo* d, J = 7.9 Hz), 7.85 (2H, C*H*(3''), d, J = 7.6 Hz), 7.75 (2H, C*H*(5'), m), 7.70 (1H, C*H*(8), dd, J = 8.5, 5.2 Hz), 7.58 (1H, C*H*(3), d, J = 5.3 Hz), 7.40 (2H, C*H*(3'), *pseudo* t, J_{app} = 6.7 Hz), 7.08 (2H, C*H*(4''), *pseudo* t, J_{app} = 7.2 Hz), 6.95 (2H, C*H*(5''), *pseudo* t, J_{app} = 7.2 Hz), 6.80 (2H, C*H*(4'), *pseudo* t, J_{app} = 6.7 Hz), 6.46 (2H, C*H*(6''), d, J = 7.4 Hz), 3.28 (2H, C*H*(δ), t, J = 7.00 Hz), 2.95 (2H, CH_2(α), t, J = 7.30 Hz), 1.82 (2H, CH_2(γ), m), 1.72 (2H, CH_2(β), m). ^{13}C NMR (D_2O, 300 K, 9.4 T): δ ppm 151.4 (CH(5)), 150.5 (CH(2)), 149.0 (CH(3')), 138.4 (CH(9)), 138.4 (CH(5')), 131.9 (CH(6'')), 130.5 (CH(5'')), 127.9 (CH(6)),

126.2 (CH(8)), 125.9 (CH(8)), 124.9 (CH(3'')), 124.1 (CH(7)), 127.9 (CH(6)), 123.3 (CH(4')), 122.6 (CH(4'')), 119.8 (CH(6')). FAB-MS: *m/z* Calcd. for $C_{38}H_{33}N_5Ir$ [M+]: 752, Found: 752 (with the expected isotopic pattern). Elemental analysis: Found = C, 57.52; H, 4.35; N, 8.73 (Calculated for $C_{38}H_{33}N_5IrCl$ = C, 57.97; H, 4.22; N, 8.89). For determining the amount of NMR silent $\mathbf{1_M}$ (i.e. $\mathbf{1_M}$ present in the form of nanoaggregates) a sample of $\mathbf{1_M}$ (1 mg ca) was dissolved in CD_2Cl_2 in a NMR tube and the intensities of its resonances were calibrated against an internal standard (CH_3CN, 1 μL). The solution was evaporated to dryness in the NMR tube, the residue was dissolved in D_2O, 1 μL of standard was added and the calibration was repeated, showing intensities of the resonances corresponding to about 75% with respect to the CD_2Cl_2 solution.

4.4. Preparation and characterization of $\mathbf{1_P}$. A water solution (2 mL) of PhenISA (57.3 mg, 7.29×10^{-3} mmol of bap) was treated with 1 mL of a THF solution containing 4.6 mg of $[Ir(ppy)_2Cl]_2$ (4.29×10^{-3}mmol, 1.15 equivalents), giving a turbid solution, which on rising the temperature to 50°C became clear. The yellow color of the solution did not change significantly during the reaction, whereas under UV illumination the orange luminescence of the complex progressively increased. After 6.5 h the mixture was concentrated under reduced pressure, to remove most of THF before purification by dialysis, performed against water with a 50 kDa cutoff dialysis tube (Spectrapore®) for 4 days at room temperature. Finally the dialyzed solution was lyophilized, affording a luminescent fluffy yellow solid. UV-Vis data (H_2O), MLCT absorptions: λ_{abs} 378 nm ($\varepsilon = 4310\ M^{-1}\ cm^{-1}$), and 417 nm ($\varepsilon = 2300\ M^{-1}\ cm^{-1}$). ^1H NMR (D_2O, 300 K, 9.4 T): Majority part signals, δ ppm 8.85 (1H, NHCO(4)), 8.75 (1H, NHCO(7)), 5.49 (1H, CH(5)), 3.49 (1H, CH_2(1)), 3.46 (1H, CH_2(12)), 3.40-3.20 (accidentally overlapped signals: 1H, CH_2(13); 1H, CH(15); 1H, CH(16)), 3.19-3.04 (accidentally overlapped signals: 1H, CH_2(1); 1H, CH(10)), 3.03 (1H, CH_2(12)), 2.87 (1H, CH_2(13)), 2.71 (1H, CH_2(16)), 2.66 (2H, CH_2(2)), 2.60 (2H, CH_2(9)). ^{13}C NMR (D_2O, 300 K, 9.4 T): δ ppm 58.2 (CH(5)), 56.4 CH(15), 55.5

CH_2(16), 52.1 CH_2(10), 49.3 CH_2(13), 48.9 CH_2(12), 48.1 CH_2(1), 30.6 CH_2(9), 30.0 CH_2(2), 13.9 CH_3(17). Elemental analysis: Found = C, 43.83; H, 6.77; N, 14.18; Ir, 2.45% (calculated for $(C_{13}H_{22}N_4O_4)_{0.94}(C_{24}H_{27}N_5O_4)_{0.06}$ $(C_{22}H_{16}ClN_2Ir)_{0.053}(H_2O)_2(CF_3SO_3H)_{0.3}$ C, 43.58; H, 6.64; N, 14.00; Ir, 2.44%). The Ir content was measured by ICP-AES spectroscopy after a known amount of lyophilized polymer was digested in a mixture of concentrated HCl and HNO_3 in 1:1 ratio for 24 h at room temperature.

4.5. Photochemical stability of $\mathbf{1_M}$ and $\mathbf{1_P}$. A sample of $\mathbf{1_P}$ (0.8 mg) was dissolved in 2.5 mL of a H_2O/MeOH 85:15 mixture (corresponding to [Ir] = 4.1×10^{-5} M). After saturation by O_2 (bubbled directly into the cuvette for 10-15 min), the solution was irradiated through a cut-off optical filter (> 390 nm) for 240 min overall, and UV-Vis absorption spectra were collected after 30, 60, 90, 180 and 240 min irradiation. The same procedure was employed for compound $\mathbf{1_M}$, in the solution obtained by dissolving 2.6 mg of **1** in 10 mL of H_2O/MeOH 85:15 mixture, and then diluting 1:10 the solution (final [$\mathbf{1_M}$] = 3.3×10^{-5}M).

4.6. Photoreaction of $\mathbf{1_M}$ and $\mathbf{1_P}$ with DHN. In a volumetric flask (10 mL) 3.2 mg of $\mathbf{1_M}$ (4.1×10^{-3} mmol) were dissolved in a mixture H_2O/MeOH 85:15 containing 6.0 mg of DHN (3.7×10^{-3} mmol). This solution was diluted 1:10 to obtain a final [$\mathbf{1_M}$] = 4.1×10^{-5} M and [DHN] = 3.7×10^{-4} M. Before irradiation the solution was saturated with O_2 by bubbling directly in the cuvette for 10 min. The solution was then irradiated through a cut-off optical filter (> 390 nm) for a total of 150 min, while spectra were recorded every 5 min during the first hour, then at 90, 120 and 150 min. The same procedure was followed for the photoreaction involving $\mathbf{1_P}$, using 0.7 mg of $\mathbf{1_P}$ (8.9×10^{-5} mmol of Ir) in 2.5 mL of the H_2O/MeOH mixture containing DHN ([**Ir**] bound to PhenISA = 3.6×10^{-5} M).

The ratio between the quantum yields for $^1O_2$ generation by $\mathbf{1_M}$ and $\mathbf{1_P}$ was evaluated on the base of the following considerations. The rate *r* of a photochemical reaction is expressed by

equation (3), where ϕ is the quantum yield of the reaction and *I* indicates the photons absorbed by the reactant.[48]

$$r = \phi I \quad (3)$$

The ratio between the quantum yields for $^1O_2$ generation is therefore given by equation 4.

$$\frac{\Phi_{\mathbf{1M}}}{\Phi_{\mathbf{1P}}} = \frac{r_{\mathbf{1M}}}{r_{\mathbf{1P}}} \times \frac{I_{\mathbf{1P}}}{I_{\mathbf{1M}}} \quad (4)$$

For monochromatic excitation the ratio $\frac{I_{\mathbf{1P}}}{I_{\mathbf{1M}}}$ can be computed by equation 5, where *I*° indicates the incident photon flux and A(**1P**) and A(**1M**) indicate the absorbance of the two complexes at the excitation wavelength.

$$\frac{I_{\mathbf{1P}}}{I_{\mathbf{1M}}} = \frac{I^{\circ}_{\mathbf{1P}}(1-10^{-\mathrm{A}(\mathbf{1P})})}{I^{\circ}_{\mathbf{1M}}(1-10^{-\mathrm{A}(\mathbf{1M})})} \quad (5)$$

In our case, multichromatic excitation by a filtered lamp was employed and then integration over the entire spectral range (λ 390-600 nm) was performed, on the reduced fraction obtained by considering that the incident photon fluxes *I*° were identical in the two experiments. The ratio $\frac{I_{\mathbf{1P}}}{I_{\mathbf{1M}}}$ so calculated resulted 0.89.

As to the $\frac{r_{\mathbf{1M}}}{r_{\mathbf{1P}}}$ term, the starting concentration of DHN was the same in the two experiments of Figure 3, and therefore the ratio between the initial reaction rates is simply given by the ratio of the k_{obs} for $\mathbf{1_M}$ and $\mathbf{1_P}$ (= 2.4). Such ratio should be poorly affected by the fact that absorbance outside the linearity range of the Lambert-Beer relationship were used in the first-order plots affording k_{obs} (Figures 2 and 3). In fact, the inaccuracy is expected to be the same in the cases of $\mathbf{1_M}$ and $\mathbf{1_P}$, because the reactant was the same (DHN) and the range of spanned absorbance was very similar in the two cases.

Therefore $\frac{\Phi_{\mathbf{1M}}}{\Phi_{\mathbf{1P}}}$ = 2.4×0.89 = 2.1.

4.7. Cells culture and treatment. The HeLa cell line[49] was cultured at 37°C with 5 % CO_2 in complete DMEM (10% FBS, 2 mM L-glutamine, 10 mM HEPES, non-essential amino acid 100 μM and penicillin plus streptomycin). Cultures at ~80% confluence were routinely split 1:10 in 10 cm culture dishes. 70-80% confluent cells were incubated with either $\mathbf{1_M}$ or $\mathbf{1_P}$ in DMEM 1% FBS. After incubation the cells were washed 3 times in PBS and then complete DMEM was added.

4.8. TPE measurements and cellular uptake. The laser source was a mode-locked Ti:sapphire laser (Mai Tai HP, Spectra Physics, CA) with pulses of 120 fs full width at half maximum and 80 MHz repetition frequency. The optical setup was built around a confocal scanning head (FV-300, Olympus, Japan) mounted on an upright optical microscope (BX51, Olympus, Japan) equipped with a high working distance objective (NA = 1.1, wd = 2 mm, 60X, water immersion, Olympus, Japan). Non-confocal TPE imaging was performed through the FV-300 scanning unit after removing the largest pinhole from the pinhole wheel. The objective simultaneously focused the laser beam on the sample and collected the signal in epi-fluorescence geometry through the non-descanned collection channels described hereafter. The non-descanned detection system (ND-unit) collected the emitted light right above the microscope objective lens, thereby avoiding the complex optical path back to the photomultipliers in the FV-300 scanning head. The signal reaching the ND-unit is fed to three Hamamatsu analog output photomultipliers (HC125-02, Hamammatsu, Japan) whose 21 mm (diameter) photocathode ensured the collection of most of the light during scanning. The ND unit has been designed to minimize the distance between the entrance pupil of the objective and the active area of the detector. The fluorescence signal was filtered by a 485/50, a 535/50 and a 600/40 band-pass filter in order to select the fluorescence light and remove either scattering or undesired auto-fluorescence from the sample, and it was processed by means of the Fluoview 5.0 software (Olympus, Japan).

Images were recorded at different times after the addition of the Ir complexes (about 2 h for $\mathbf{1_M}$, 100 μL of a 5.5×10^{-4} M solution, affording a 26 μM concentration in the well; about 12 h for $\mathbf{1_P}$, 100 μL of a 4.7×10^{-4} M solution, affording a 22 μM concentration in the well). Two photon excitation at 840 nm was exploited (with an excitation power of 15 mW). The bleed through of autofluorescence was verified on non-stained samples by measuring the fluorescence emission in the presence and in the absence of the band pass filter selecting the emission of the samples. Images shown in the paper are the result of 2 kalman average scans with 10 or 6 μs of residence time per pixel, depending on the zoom factor. The field of view of the 512x512 pixel images was 157x157 μm^2 or 79x79 μm^2, as indicated in the caption of Figure 4.

4.9. Flow cytometry. 4h and 6h after treatment, the adherent cells were harvested from the culture dishes with trypsin-EDTA (euroclone) and then collected in complete DMED, washed 3 times in FACS buffer (FACS = Fluorescence-activated-cell-sorting) containing Phosphate Buffer Solution (PBS) with 2 mM EDTA and 2% Fetal Bovine Serum (FBS) and then processed for annexin V / 7ADD assay (biolegend, San Diego, CA. USA) following the manufacturer's instructions. Stained cells (about 5×10^4) were acquired with CANTO II flow cytometer (BD Pharmingen) and analyzed with FlowJo software (Treestar).

4.10 Viability test in the dark. HeLa cells (at 80% of confluency) were cultured and treated with $\mathbf{1_M}$ or $\mathbf{1_P}$ as described in paragraph 4.7 and then trypan blue exclusion test (that selectively stained the dead cells) and Neubauer cell counting chamber were used to count the total cells number and the % of dead cells. All conditions were done in triplicate.

ASSOCIATED CONTENT

Supporting Information. The NMR spectra, the absorption and emission data in different solvents, the DLS size distribution profile, the stability test, the microscopy image of the control

untreated HeLa cells, the flow-cytometry analysis, the dark toxicity data, and the emission profile of the Xe lamp. This material is available free of charge via the Internet at http://pubs.acs.org.

AUTHOR INFORMATION

Corresponding Author

*e-mail: *daniela.maggioni@unimi.it* . Fax: +390250314405. Phone: +390250314352

ACKNOWLEDGMENT

The authors warmly thank Dr. Vladimiro Dal Santo for ICP-AES measurements.

Table of Contents Graphic and Synopsis

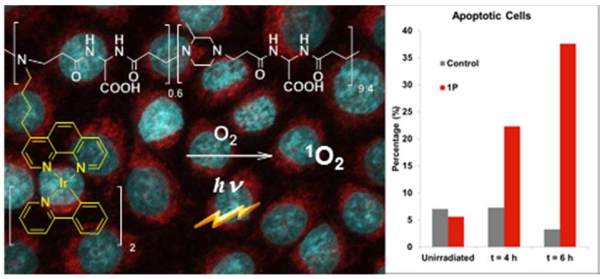

Luminescent $[Ir(ppy)(phen)]^+$ complexes appended to a water soluble poly(amidoamine) copolymer show longer lifetimes of their triplet excited states and higher photoluminescence quantum yields than the free complexes, and maintain the capability to sensitize $^1O_2$ generation. The Ir-functionalized poly(amidoamine) is able to penetrate the cellular membrane of HeLa cells, acting as two-photon-excitation imaging agent and as effective sensitizer for cell photodynamic therapy. Moreover, the binding to the polymer avoids the cell damage induced by the free Ir complexes.

REFERENCES

(1) (a) DeRosa, M. C.; Crutchley, R. J. *Coord. Chem. Rev.* **2002**, *233-234*, 351–371; (b) Wang, S.; Gao, R.; Zhou, F.; Selke, M. *J. Mater. Chem.* **2004**, *14*, 487–493; (c) Allison, R. R.; Mota, H. C.; Shibata, C. H. *Photodiag. Photodyn. Ther.* **2004**, *1*, 263–277; (d) Chatterjee, D. K.; Fong, L. S.; Zhang, Y. *Adv. Drug Deliv. Rev.* **2008**, *60*, 1627–1637.

(2) Triesscheijn, M.; Baas, P.; Schellens, J. H.; Stewart, F.A. *Oncologist* **2006**, *11*, 1034–1044.

(3) Rhodes, L. E.; de Rie, M.; Enstrom, Y.; Groves, R.; Morken, T.; Goulden, V.; Wong, G. A.; Grob, J. J.; Varma, S.; Wolf, P. *Arch. Dermatol.* **2004**, *140*, 17–23.

(4) Hur, C.; Nishioka, N. S.; Gazelle, G. S. *Dig. Dis. Sci.* **2003**, *48*, 1273–1283.

(5) Kato, H. *J. Photochem. Photobiol.* **1998**, *B 42*, 96–99.

(6) Schuller, D. E.; McCaughan, Jr J. S.; Rock, R. P. *Arch. Otolaryngol.* **1985**, *111*, 351–355.

(7) Kharkwal, G. B.; Sharma, S. K.; Huang, Y. Y.; Dai, T; Hamblin, M. R. *Lasers Surg. Med.* **2011**, *43*, 755–767.

(8) Agostinis, P.; Berg, K.; Cengel, K. A.; Foster, T. H.; Girotti, A. W.; Gollnick, S. O.; Hahn, S. M.; Hamblin, M. R.; Juzeniene, A.; Kessel, D.; Korbelik, M.; Moan, J.; Mroz, P.; Nowis, D.; Piette, J.; Wilson, B. C.; Golab, J. *CA Cancer J. Clin.* **2011**, *61*, 250–281.

(9) See for instance (a) Mroz, P; Yaroslavsky, A; Kharkwal, G. B.; Hamblin, M. R. *Cancers* **2011**, *3*, 2516-2539; (b) Allison, R. R.; Moghissi, K. *Clin. Endosc.* **2013**, *46*, 24-29

(10) Oleinick, N. L.; Morris, R. L.; Belichenko, I. *Photochem. Photobiol. Sci.*, **2002**, *1*, 1–21, and refs therein.

(11) (a) Murtinho, D.; Pineiro, M.; Pereira, M.; d'A. Gonsalves, A. M.; Arnaut, L. G.; Miguel M. G.; Burrows, H. D. *J. Chem. Soc. Perkin Trans.* **2000**, *2*, 2441–2447; (b) Horiuchi, H.; Tanaka, T.; Yoshimura, K.; Sato, K.; Kyushin, S.; Matsumoto, H.; Hiratsuka, H. *Chem. Lett.* **2006**, *35*, 662–663; (c) Maeda, D.; Shimakoshi, H.; Abe, M.; Hisaeda, Y. *Inorg. Chem.* **2009**, *48*, 9853–9860.

(12) (a) Ikeda, A.; Sato, T.; Kitamura, K.; Nishiguchi, K.; Sasaki, Y.; Kikuchi, J.; Ogawa, T.; Yogo, K.; Takeya, T. *Org. Biomol. Chem.* **2005**, *3*, 2907–2909; (b) Mroz, P.; Tegos, G. P.; Gali, H.; Wharton, T.; Sarna T.; Hamblin, M. R. *Photochem. Photobiol. Sci.* **2007**, *6*, 1139–1149.

(13) Tardivo, J. P.; Giglio, A. D.; Oliveira, C. S.; Gabrielli, D. S.; Junqueira, H.C.; Tada, D. B.; Severino, D.; Turchiello, R. F.; Baptista, M. S. *Photodiag. Photodyn. Ther.* **2005**, *2*, 175–191.

(14) Ishiyama, K.; Nakamura, K.; Ikai, H.; Kanno, T.; Kohno, M.; Sasaki, K.; Niwano, Y. *PLoS One* **2012**, *7*, e37871.

(15) Takizawa, S.; Aboshi, R.; Murata, S. *Photochem. Photobiol. Sci* **2011**, *10*, 895–903.

(16) (a) Djurovich, P. I.; Murphy, D.; Thompson, M. E.; Hernandez, B.; Gao, R.; Hunt, P. L.; Selke, M. *Dalton Trans.* **2007**, 3763–3770; (b) Gao, R.; Ho, D. G.; Hernandez, B.; Selke, M.; Murphy, D.; Djurovich, P. I.; Thompson, M. E. *J. Am. Chem. Soc.* **2002**, *124*, 14828–14829.

(17) (a) Majumdar, P.; Yuan, X.; Li, S.; Le Guennic, B.; Jie Ma, J.; Zhang, C.; Jacqueminde, D.; Zhao, J. *J. Mater. Chem. B* **2014**, *2*, 2838–2854; (b) Nakagawa, A.; Hisamatsu, Y.;

Moromizato, S.; Kohno, M.; Aoki, S. *Inorg. Chem.* **2014**, *53*, 409−422; (c) Ye, R.-R.; Tan, C.-P.; He, L.; Chen, M.-H.; Ji, L.-N.; Mao, Z.-W. *Chem. Commun.* **2014**, *50*, 10945−10948; (d) Li, S. P.-Y.; Lau, C. T.-S.; Louie, M.-W.; Lam, Y.-W.; Cheng, S. H.; Lo, K. K.-W. *Biomaterials* **2013**, *34*, 7519–7532; (e) Moromizato, S.; Hisamatsu, Y.; Suzuki, T.; Matsuo, Y.; Abe, R.; Aoki, S. *Inorg. Chem.* **2012**, *51*, 12697−12706.

(18) Sajoto, T.; Djurovich, P. I.; Tamayo, A. B.; Oxgaard, J.; Goddard, W. A.; Thompson, M. E. *J. Am. Chem. Soc.* **2009**, *131*, 9813–9822.

(19) (a) Larson, N.; Ghandehari, H. *Chem. Mater*. **2012**, *24*, 840−853; (b) Soesbe, T. S.; Kiefer, G. E.; Sherry, A. D. *J. Am. Chem. Soc*. **2008**, *130*, 13854−13855; (c) Liu, L.; Li, X.; Hou, S.; Xue, Y.; Yao, Y.; Ma, Y.; Feng, X.; He, S.; Lu, Y.; Wang, Y.; Zeng, X. *Chem. Commun.* **2009**, *44*, 6759−6761; (d) Kim, J. H.; Park, K.; Nam, H. Y.; Lee, S.; Kim, K.; Kwon, I. C. *Prog. Polym. Sci.* **2007**, *32*, 1031−1053.

(20) (a) Matzumura, Y.; Maeda, H. *Cancer Res.* **1986**, *46*, 6387–6392; (b) Fox, M. E.; Szoka, F. C.; Fréchet, J. M. *Acc. Chem. Res.* **2009**, *42*, 1141−1151; (c) Peer, D.; Karp, J. M.; Hong, S.; Farokhzad, O. C.; Margalit, R.; Langer, R. *Nat. Nanotechnol*. **2007**, *2*, 751−760.

(21) (a) Ferruti, P.; Marchisio, M. A.; Duncan, R. *Macromol. Rapid Commun.* **2002**, *23*, 332−355; (b) Ranucci, E.; Ferruti, P.; Lattanzio, E.; Manfredi, A.; Rossi, M.; Mussini, P. R.; Chiellini, F.; Bartoli, C. *J. Polym. Sci., Part A: Polym. Chem.* **2009**, *47*, 6977−6991.

(22) (a) Cavalli, R.; Bisazza, A.; Sessa, R.; Primo, L.; Fenili, F.; Manfredi, A.; Ranucci, E.; Ferruti, P. *Biomacromolecules* **2010**, *11*, 2667−2674. (b) Ferruti, P.; Franchini, J.; Bencini, M.;

Ranucci, E.; Zara, G. P.; Serpe, L.; Primo, L.; Cavalli, R. *Biomacromolecules* **2007**, *8*, 1498−1504.

(23) Donghi, D.; Maggioni, D.; D'Alfonso, G.; Amigoni, F.; Ranucci, E.; Ferruti, P.; Manfredi, A.; Fenili, F.; Bisazza, A.; Cavalli, R. *Biomacromolecules* **2009**, *10*, 3273−3282.

(24) Maggioni, D.; Fenili, F.; D'Alfonso, L.; Donghi, D.; Panigati, M.; Zanoni, I.; Marzi, R.; Manfredi, A.; Ferruti, P.; D'Alfonso, G.; Ranucci, E. *Inorg. Chem.* **2012**, *51*, 12776−12788.

(25) Richardson, S.; Ferruti, P.; Duncan, R. *J. Drug Targeting* **1999**, *6*, 391−404.

(26) Lowry, M. S.; Hudson, W. R.; Pascal, R. A. Jr.; Bernhard, S. *J. Am. Chem. Soc*. **2004**, *126*, 14129−14135.

(27) Wang, Z.; McWilliams, A. R.; Evans, C. E. B.; Lu, X.; Chung, S.; Winnik, M. A.; Manners, I. *Adv. Funct. Mater*. **2002**, *12*, 415−419.

(28) Zhao, Q.; Liu, S.; Shi, M.; Li, F.; Jing, H.; Yi, T.; Huang, C. *Organometallics* **2007**, *26*, 5922−5930.

(29) The term solvent's "polarity" is usually employed for describing the capacity of a solvent for solvating dissolved charged or dipolar species.[30] Although easy to qualitatively understand, substantial difficulties are encountered on attempting a more precise/comprehensive definition of "polarity" or its quantitative measure. Many semiempirical solvent polarity scales have been developed,[30] and some of them are derived from spectroscopic measurements, such as the well known $E_T(30)$ scale.[31]

(30) Katritzky, A. R.; Fara, D. C.; Yang, H.; Tämm, K.; Tamm, T.; Karelson, M. *Chem. Rev.* **2004**, *104*, 175−198.

(31) Reichardt, C. *Solvents and Solvent Effects in Organic Chemistry*, Wiley-VCH Publishers, Weinheim, 3rd ed., **2003**.

(32) Giordano P. J.; Wrighton, M. *J. Am. Chem. Soc.* **1979**, *101*, 2888−2897.

(33) Lakowicz, J. R. *Principles of Fluorescence Spectroscopy*, **1999**, Kluwer Academic/Plenum Publishers, New York, II Ed., Ch. 6, p. 185.

(34) Lo, K. K.-W.; Ng, D. C.-M.; Chung, C.-K. *Organometallics* **2001**, *20*, 4999–5001, and references therein.

(35) See for instance Mauro, M.; De Paoli, G.; Otter, M.; Donghi, D.; D'Alfonso, G.; De Cola, L. *Dalton Trans.* **2011**, *40*, 12106–12116.

(36) See for instance Rampazzo, E.; Bonacchi, S.; Montalti, M.; Prodi, L.; Zaccheroni, N. *J. Am. Chem. Soc*. **2007**, *129*, 14251–14256.

(37) Yersin, H.; Rausch, A. F.; Czerwieniec, R.; Hofbeck, T.; Fischer, T. *Coord. Chem. Rev.* **2011**, *255*, 2622–2652.

(38) Wrighton, M.; Morse, D. L. *J. Am. Chem. Soc*. **1974**, *96*, 998–1003.

(39) See for instance (a) Lees, A. J. *Coord. Chem. Re*v. **1998**, *177*, 3–35; (b) Li, M.-J.; Chen, Z.; Yam, V. W.-W., Zu, Y. *ACS Nano* **2008**, *2*, 905–912.

(40) Wu, W.; Yang, P.; Ma, L.; Lalevée, J.; Zhao J. *Eur. J. Inorg. Chem.* **2013**, 228−231.

(41) Stratakis, M.; Orfanopoulos, M. *Tetrahedron* **2000**, *56*, 1595–1615.

(42) (a) Fernandez-Moreira, V.; Thorp-Greenwood, F. L.; Coogan, M. P. *Chem. Commun.* **2010**, *46*, 186–202; (b) Mari, C.; Panigati, M.; D'Alfonso, L.; Zanoni, I.; Donghi, D.; Sironi, L.; Collini, M.; Maiorana, S.; Baldoli, C.; D'Alfonso, G.; Licandro, E. *Organometallics* **2012**, *31*, 5918−5928.

(43) Lo, K. K.-W.; Lee, P.-K.; Lau, J. S.-Y. *Organometallics* **2008**, *27*, 2998–3006.

(44) Strassert, C. A.; Mauro, M.; De Cola, L. *Adv. Inorg. Chem.* **2011**, *63*, 47–103.

(45) Ferruti, P.; Ranucci, E.; Trotta, F.; Gianasi, E.; Evagorou, G. E.; Wasil, M.; Wilson, G.; Duncan, R. *Macromol. Chem. Phys.* **1999**, *200*, 1644−1654.

(46) Sprouse, S.; King K., A.; Spellane, P. J.; Watts, R. J. *J. Am. Chem. Soc*. **1984**, *106*, 6647−6653.

(47) Ishida, A.; Tobita, S.; Hasegawa, Y.; Katoh, R.; Nozaki, K. *Coord. Chem. Rev*. **2010**, *254*, 2449−2458.

(48) Balzani, V.; Carassiti, V. *Photochemistry of Coordination Compounds*, Academic Press: London and New York, **1970**.

(49) Scherer, W. F.; Syverton, J. T.; Jey, G. O. *J. Exp. Med.* **1953**, *97*, 695–710.